# Computer simulation evidence of the transient planar state during the homeotropic to focal conic transition in cholesteric liquid crystals

J. E. Anderson, P. Watson, T. Ernst, and P. J. Bos
*Liquid Crystal Institute, Kent State University, Kent Ohio 44242*
(Received 1 April 1999; revised manuscript received 29 September 1999)

Previous experimental evidence has suggested the existence of a transient planar state during the transition from a homeotropic state to a focal conic state. This does not appear at first to be physically reasonable. Here we show a quantitative numerical model of this transition that shows the existence of the transient planar state and agrees well with measured data. We compared this simulation with two experimental samples: one with parallel boundary conditions, and one with perpendicular boundary conditions. Both samples had thickness to pitch ratios of 13.9. The agreement of the simulation with the experimental data gives further evidence that the system passes through the transient planar during the transition. Also shown here are preliminary results for the second part of the transition, the transition from the transient planar state to the focal conic state, that suggest a Helfrich-like undulation deformation.

PACS number(s): 61.30.−v, 78.20.Bh, 78.20.Jq, 83.70.Jr

## I. INTRODUCTION

The cholesteric phase is a liquid crystal phase in which the liquid crystal director (the average orientation of the long axis of the molecule) rotates in space about some axis [1]. The distance for the director to spatially twist 360° is defined as the pitch $P$. The unstrained (intrinsic) pitch is called $P_0$, with wave vector $q_0(=2\pi/P_0)$. This periodicity causes Bragg reflection of light with peak wavelength $\lambda_{\max}=\langle n\rangle P_0$, and of spectral width $\Delta\lambda=\Delta n P_0$ [1]. Here $\langle n\rangle$ is the average index of refraction, and $\Delta n$ is the birefringence of the material.

If a chiral dopant (a material that lacks mirror symmetry) is mixed with a nematic liquid crystal host, the director of the nematic can be made to rotate [2]. The pitch of the mixture can be controlled precisely by varying the concentration of the chiral dopant [2]. If the correct amount of dopant is added, the material can be made to reflect light in the visible spectrum [2].

In the confined geometry of a liquid crystal cell, cholesteric material can exist in a number of textural states. The planar ($P$) state is obtained when the helical axes are pointing approximately perpendicular to the substrates and the pitch is unstrained. The homeotropic ($H$) state, (also called the field-induced nematic state), is characterized by the directors being approximately aligned with one another as in a nematic, and pointing perpendicular to the substrates [1]. In cells with $d/P_0 > K_{33}/2K_{22}$ (typically $\approx 1$), the $H$ state can only be achieved by applying a sufficiently large external field [3]. For the purposes of this study, an electric field was used to induce this state. To achieve the transition from a twisted structure to the $H$ state, the field must be above the critical value, $E_{CN}$, given in Eq. (1) [1]. Greubel derived the field required to drop from the $H$ state to a twisted state, assuming homeotropic boundary conditions, which is given in equation (2) [3]:

$$E_{CN}=\left(\frac{\pi^2}{P_0}\right)\left(\frac{K_{22}}{\varepsilon_0\Delta\varepsilon}\right)^{1/2}, \tag{1}$$

$$E_{NC}=\left(\frac{\pi}{P_0}\right)\left(\frac{4K_{22}^2-\left(\frac{P_0K_{33}}{d}\right)^2}{\varepsilon_0\Delta\varepsilon K_{33}}\right)^{1/2}. \tag{2}$$

In the focal conic (FC) state, the directors exhibit an intrinsic twist about some axis, with the axis approximately parallel to the substrates [1]. If the system is in the $H$ state, and the field is reduced to a value of roughly $E_{NC}$ the system will transform from the $H$ state to the FC state [3,4]. Yang and Liu gave experimental results suggesting the existence of the transient planar (TP) state in the transition from the $H$ state to the FC state at some voltages [4]. The TP state is similar to the $P$ state in that the helical axes are aligned approximately along the substrate normal, however it has a longer pitch ($P^*\sim P_0K_{33}/K_{22}$) [4]. However, it does not appear physically correct for the system to pass through the TP state. It would seem easier for the system to go directly to the FC state. In this paper, we show that quantitative numerical simulation indeed shows the system passing through the TP state.

## II. NUMERICAL SIMULATIONS

The method used to calculate the director structure of the liquid crystal system is based on the fact that nature acts to minimize the free energy of the system. The expression for the free energy density of a liquid crystal system in terms of the director, $\mathbf{n}$, is given by Eq. (3) [1]:

$$f=\tfrac{1}{2}K_{11}(\boldsymbol{\nabla}\cdot\hat{\mathbf{n}})^2 + \tfrac{1}{2}K_{22}(\hat{\mathbf{n}}\cdot\boldsymbol{\nabla}\times\hat{\mathbf{n}}+q_0)^2+\tfrac{1}{2}K_{33}|(\hat{\mathbf{n}}\times\boldsymbol{\nabla}\times\hat{\mathbf{n}})|^2-\tfrac{1}{2}\mathbf{D}\cdot\mathbf{E}. \tag{3}$$

Here $K_{11}$, $K_{22}$, and $K_{33}$ are the elastic constants for splay, twist and bend, respectively, $\mathbf{D}$ is the electric displacement and $\mathbf{E}$ is the electric field.

During the initial stages of the transition from the $H$ state to the FC state, the data as shown below suggests a one-dimensional transition. However, because the director is so

 

tightly twisted, we did not want to restrict the simulations so strenuously. For this reason, and because we desired information on the latter part of the transition, we allowed the system to vary over two spatial dimensions.

It has been found that writing this free energy as a function of the order parameter tensor **Q**, instead of the director **n**, when calculating director configurations can cause nonphysical results [5]. This is because the **n** and $-\mathbf{n}$ equivalence can cause the tensor approach to calculate a low energy when an elastic deformation slips completely between two adjacent grid points, forcing the two directors to point in opposite directions [5]. This problem is especially relevant here, where it is possible for defects to form in such high energy areas. For these reasons, the vector approach was employed here.

Ignoring flow of the director, the dynamics of the director reorientation can be calculated by setting the functional derivatives of the free energy density with respect to each director component (the elastic torque) equal to the rotational torque on that component as shown in Eq. (4) [6]:

$$\gamma_1 \frac{dn_i}{dt} = -\frac{\delta f}{\delta n_i} + \lambda n_i, \quad i = x,y,z, \tag{4}$$

where $\gamma_1$ is the rotational viscosity. In two dimensions,

$$\frac{\delta f}{\delta n_i} = \frac{\partial f}{\partial n_i} - \frac{d}{dx}\left(\frac{\partial f}{\partial \frac{dn_i}{dx}}\right) - \frac{d}{dz}\left(\frac{\partial f}{\partial \frac{dn_i}{dz}}\right), \quad i = x,y,z. \tag{5}$$

In Eq. (4), the Lagrange multiplier $\lambda$ is used to maintain the unit length of the director. However, we cannot simultaneously solve this equation for the Lagrange multiplier and a numerical update formula for $n_i$. Therefore, the $\lambda$term is dropped, and **n** is renormalized to have unit length after each time step, i.e., each director component is divided by the total length [7,8].

Because the dielectric constant is anisotropic, the electric potential at each point depends on the director orientation at that and surrounding points. When Maxwell's equation $\nabla \cdot \mathbf{D} = 0$, is discretized, an equation linear in these values results [8]. This can then be solved to yield a numerical update equation for the potential at the current grid point in terms of the neighboring values of potential and director components.

In order to calculate dynamics of the system, the new director field on the entire computational grid must be calculated before any variables are updated. This ensures that all directors are at the same time step when derivatives are calculated. After the director field has been calculated and the new values stored into the arrays, the new electric potential at each point can be calculated.

If the initial director configuration used in simulation is exactly $\mathbf{n} = (0,0,1)$ everywhere, we found the calculation to be in a metastable equilibrium when homeotropic boundary conditions were used. To avoid this, we started both calculations with some amount of random noise. The initial director configurations were calculated by first setting $n_x$ and $n_y$ to random numbers between $-0.25$ and 0.25 then using the relation $n_z = \mathrm{sqrt}(1 - n_x^2 - n_y^2)$ (derived from the unit length of the director) to determine $n_z$. One can qualitatively think of this noise as related to thermal director fluctuations. However, we have found that the amplitude of this random noise affects the director configurations very little.

To include the effect of the large percentage (40%) of chiral additive (CB15 from Merck) in the system on the elastic constants, we followed the report of Ref. [9] to estimate the elastic constants in our system. These authors experimentally measured the elastic constants of a mixture as a function of weight percentage when both enantiomers of CB15 were added to a nematic host. The authors found reductions of 61.5%, 58.8%, and 48.6% for $K_{11}$, $K_{22}$, and $K_{33}$ respectively. We can include this effect by reducing the elastic constants of our system by these same percentages. For this study, we used MLC 6080 from Merck as the nematic host. We chose this material for its large birefringence ($\Delta n = 0.2024$) and low viscosity ($\gamma_1 \approx 0.133$). The values of the elastic constants for our system were thus adjusted from 14.4, 7.1, and 19.1 pN to 8.86, 4.17, and 9.28 pN for $K_{11}$, $K_{22}$, and $K_{33}$ respectively.

This drop in elastic constants with chiral concentration can be compared to the drop in elastic constants with temperature found by the same authors [9]. This comparison yields an effective temperature increase of roughly 25°.

To our knowledge, no work has been done investigating the effect of chiral concentration on the rotational viscosity. However, the rotational viscosity is only used to scale time in simulations; therefore, we may rescale time to coincide with the data. Similarly, no work has been done to the authors' knowledge of the effects of the chiral additive on the dielectric constants or refractive indices. The dielectric constants can be determined experimentally from capacitance measurements. We let the planar cell relax into the perfect planar over a period of a few days. Then we measured the capacitance using 0.1 V as the probing voltage. From this we measured $\varepsilon_\perp$ to be $5.51 \pm 0.05$. To measure $\varepsilon_\parallel$, we applied a high probing voltage (50 V) to the homeotropic sample and measured the capacitance. This yielded a value of $14.31 \pm 0.5$ for $\varepsilon_\parallel$. To determine the indices of refraction, we used a weighted average of the host and the chiral values. The refractive indices have never been measured for CB15; however, the chemical structure of CB15 is very similar to the nematic 5CB, with the exception that CB15 has a chiral center in the alkyl chain [10]. Therefore, these values were used when calculating the average [11]. The indices of refraction for the nematic host are 1.7100 and 1.5076 for the extraordinary and ordinary indices of refraction. For 5CB, these values are 1.7212 and 1.5376, yielding weighted averages of 1.7145 and 1.5196.

For the purposes of this study, we assumed the scalar order parameter $S$ to be constant in space. This simplification does not allow for defects having an isotropic core. The validity of this assumption was tested by comparing the free-energy density at every lattice point with the free-energy density of a defect core. This assumes that the free-energy density is constant between grid points. This assumption can only introduce a small error due to the fact that the grid spacing is not much larger than a molecular length. The grid spacing is $5\ \mu\mathrm{m}/197 = 25.4\ \mathrm{nm}$, and a molecular lengths for standard nematic liquid crystals are on the order of 10-nm [1]. The free energy of a defect core should be on the order

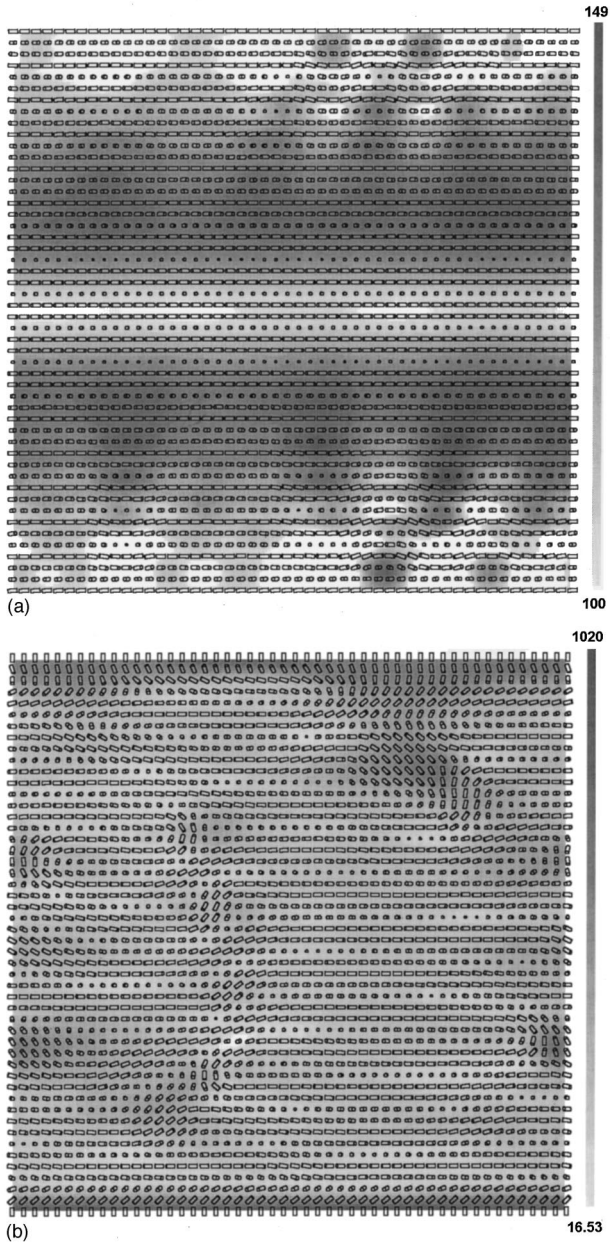


FIG. 1. Example of free energy density calculations for (a) the planar sample and (b) the homeotropic sample.

of $Kl_0$, where $K$ is an average elastic constant and $l_0$ is a molecular length [1]. This core has a length scale on the order of a molecular length [1]. Therefore, the free energy density of a defect core should be roughly $K/l_0^2$. For our system, this free energy density evaluates to roughly 75,800 $\mathrm{J\,m^{-3}}$. If this free energy density is always less than the free energy density found in calculations, no defects will form. Using these numbers, we found the free energy density to always be at least a factor of 50 times smaller than that required for defects to form, with the highest values occurring at the homeotropic boundaries. Two such calculations showing this free energy density and director configurations are shown in Fig. 1. Figure 1(a) shows a typical energy density diagram for the calculation with rubbed planar boundaries, and Fig. 1(b) shows a typical energy density diagram for the calculation with homeotropic boundary conditions.

The director configurations during the early stages of the transition from the $H$ state to the FC state are shown in Figs. 2 and 3. Figure 2 shows the transition for the sample with rubbed planar boundary conditions, while Fig. 3 shows the director configuration as a function of time for the homeotropic boundary condition sample. These figures are downsampled from a $197\times197$ computational grid. In all simulations done here, the thickness in the $x$ direction was kept the same as in the $z$ direction, which was 5.0 $\mu$m.

For this simulation, we used periodic boundary conditions in the $x$ and $y$ directions. During the initial stages of the transition, the system transforms through a one-dimensional conical relaxation. Thus, during this part of the transition, the periodic boundary conditions have no effect on the results. The preliminary results for the transition from the TP state to the FC state show feature sizes much smaller than 5 $\mu$m, thus indicating that the periodic boundary conditions have little or no effect. We have performed this calculation for other values of thickness to pitch ratio, and found very little dependence, also suggesting the periodic boundary conditions have little or no effect.

## III. EXPERIMENT

To verify the accuracy of the simulation, we prepared two samples, one with strong planar anchoring at the boundaries and the other with strong perpendicular (homeotropic) anchoring at the boundaries. The planar boundary conditions were achieved by spin coating an organic polyimide (Dupont 2555) which was then rubbed with a felt cloth. The pretilt angle in a sample filled with the nematic host was measured by the magnetic null method to be $(3.75\pm0.5)°$. The homeotropic boundary conditions were achieved by spin coating a strong homeotropic surfactant (Aldrich Octadecyltrichlorosilane, which we will refer to as ''silane''). By mixing 40% by weight of chiral (CB15 from Merck) with a nematic host (MLC 6080 from Merck) we were able to obtain a reflection in the visible region.

The method used to measure the pitch of the material uses the relation between the reflected spectrum and the pitch, $\lambda_{\max}=\langle n\rangle P_0$. From the average indices of refraction given above, we obtain an $\langle n\rangle$ for the mixture of 1.6170. If the planar sample is allowed to relax into the $P$ state for a few hours, the ''perfect'' $P$ state appears. This state has nearly all reflecting helices aligned perpendicular to the substrates [12]. By measuring the reflectance spectrum for the perfect $P$ state in the planar sample, the wavelength of peak reflectance was found to be $580\pm10$ nm. This yields a $P_0$ of 358.7 $\pm6.2$ nm. The measured reflection spectrum is shown in Fig. 4. The sample thicknesses were controlled by 5-$\mu$m glass cylinders and were measured by interference methods to be $5.0\pm0.2$ $\mu$m for both samples. This gives a thickness to pitch ratio $(d/P_0)$ of $13.9\pm0.6$. This value was used in the simulations.

The critical voltage to obtain the $H$ state can be calculated by multiplying Eq. (1) by the sample thickness. The critical voltage in our system was approximately 30 V. In the experiments performed here, the voltage applied to obtain the $H$ state was always greater than or equal to 50 V to ensure that the $H$ state was fully realized. To allow the system to transform to the FC state, it is necessary to drop the voltage from

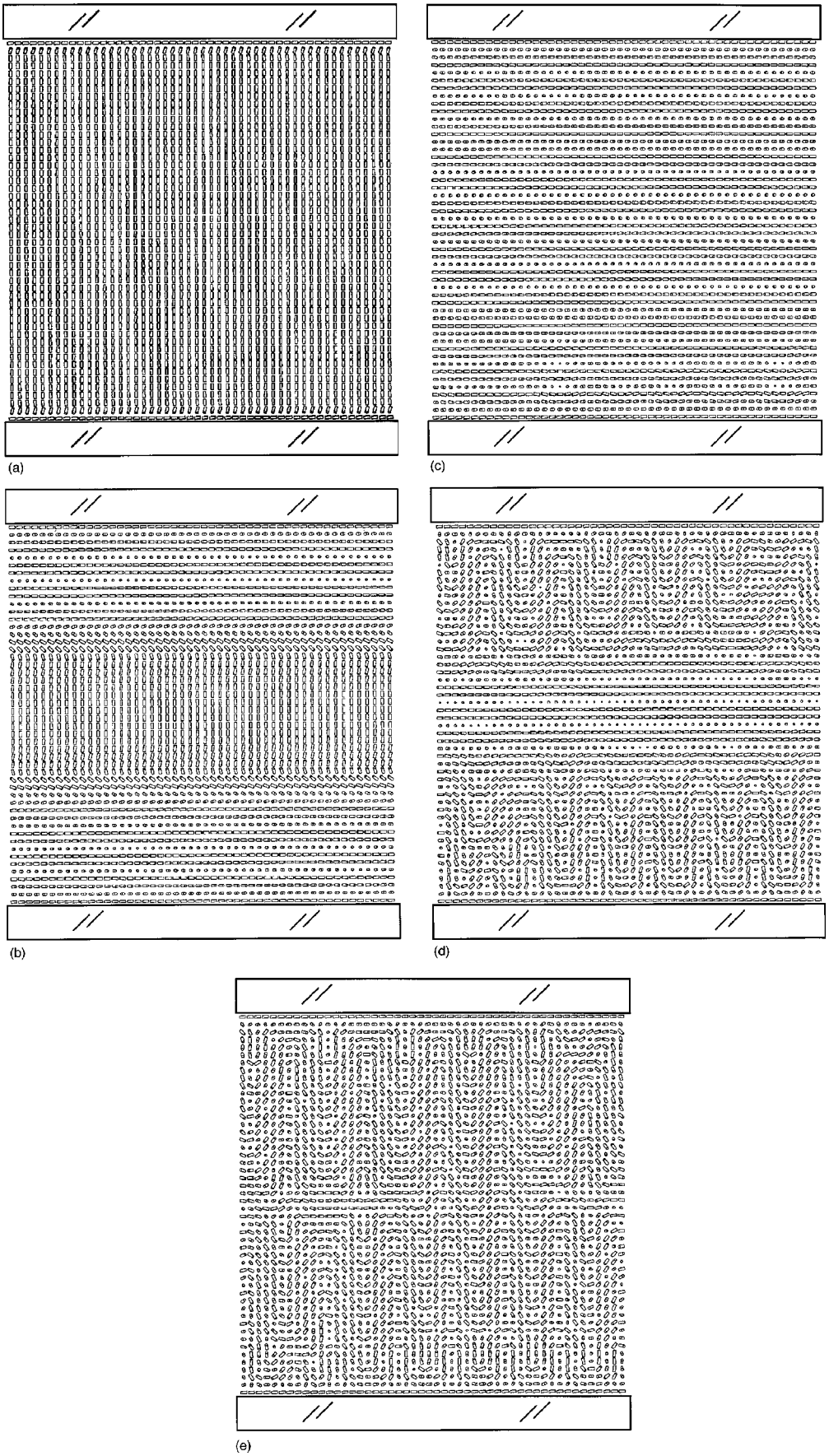


FIG. 2. Simulated director configuration during the transition from the homeotropic state to the focal conic state for the planar sample. Times are (a) 0.03, (b) 1.03, (c) 1.52, (d) 3.03, and (e) 4.55 ms. Substrates are shown for clarity.

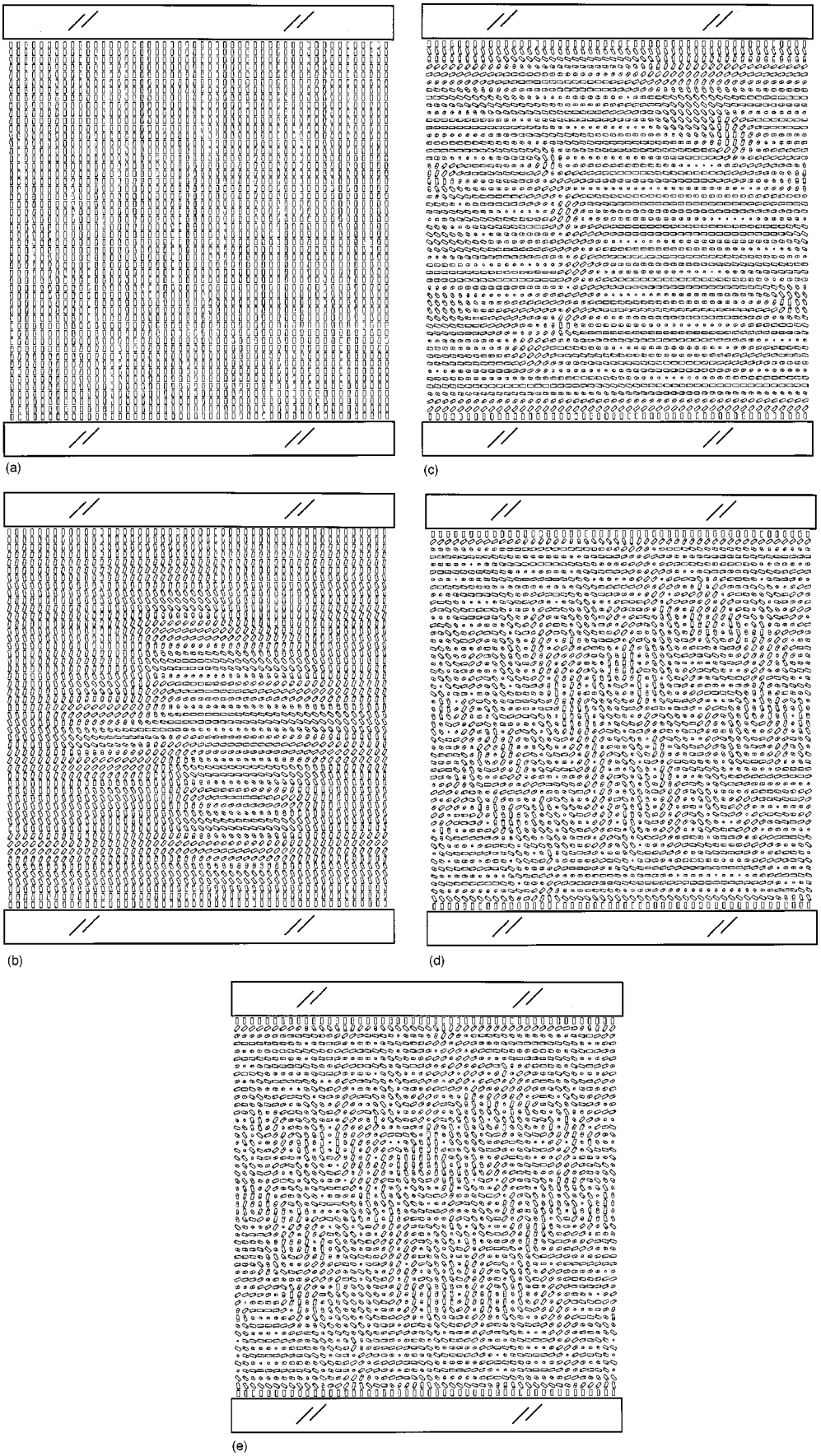


FIG. 3. Simulated director configuration during the transition from the homeotropic state to the focal conic state for the homeotropic sample. Times are (a) 0.03, (b) 0.606, (c) 1.03, (d) 3.03, and (e) 4.55 ms. Substrates are shown for clarity.

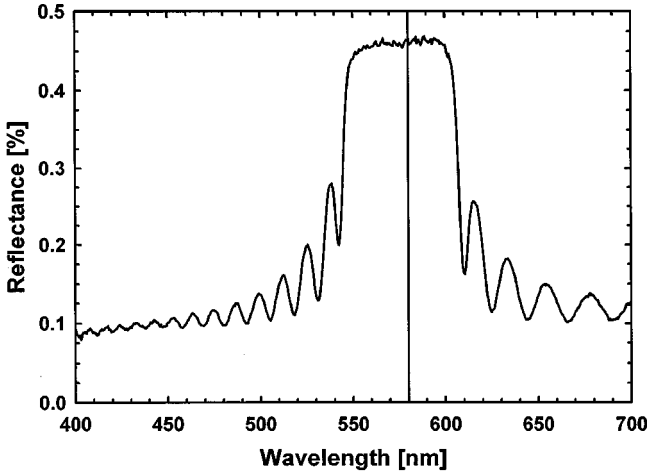


FIG. 4. Measured reflectance spectrum from the ''perfect'' planar structure in the planar sample.

the $H$ state value not to zero, but to an intermediate bias voltage. Equation (2) can be used to determine the correct value of the bias. For our system, this yields a voltage of roughly 13 V, agreeing well with our experimental values of 15 V for the rubbed planar sample and 10 V for the homeotropic sample. These experimental values were also used in calculations.

Three experiments were performed to verify the numerical simulations. First we measured the capacitance of the samples as a function of time. This can be accomplished by connecting a known capacitance $C_0$, in series with the sample and measuring the voltage across the known capacitance as a function of time [13]. The equation for the capacitance of the sample is derived in Eq. (6). We ensured $C_0 \gg C_{\mathrm{LC}}$, so that the voltage drop across the liquid crystal sample was very close to the applied voltage. When performing this experiment, the frequency must be low enough to allow full charging of the system to obtain quantitatively correct capacitance values. In our experiment, the value of $C_0$ was 0.455 $\mu$F, and the driving frequencies were 4 and 10 kHz for the planar sample and the homeotropic sample respectively:

$$\frac{V_{\mathrm{measured}}}{V_{\mathrm{applied}}}=\frac{C_{\mathrm{total}}}{C_0}, \quad \frac{1}{C_{\mathrm{total}}}=\frac{1}{C_0}+\frac{1}{C_{\mathrm{LC}}},$$
$$C_{\mathrm{total}}=\frac{C_0 C_{\mathrm{LC}}}{C_0+C_{\mathrm{LC}}}\cong C_{\mathrm{LC}}, \Rightarrow C_{\mathrm{LC}}\cong C_0\frac{V_{\mathrm{measured}}}{V_{\mathrm{applied}}}. \tag{6}$$

The capacitance of a dielectric sample between two conducting plates is given by Eq. (7).

$$C=\varepsilon\varepsilon_0 A/d_Z, \tag{7}$$

where $\varepsilon$ is the relative permittivity or dielectric constant, $\varepsilon_0$ is the permittivity of free space ($8.85\times10^{-12}\,\mathrm{F\,m^{-1}}$ in MKS units), $A$ is the area of the plates, and $d_Z$ is the spacing between the plates, in this case the sample thickness. However, as noted before, the dielectric constant of a liquid crystal system is anisotropic, and therefore depends on director orientation. Hence an average dielectric constant, given by Eq. (8), must be used,

$$\bar{\varepsilon}=\frac{1}{N_X}\sum_X \frac{1}{\frac{1}{N_Z}\sum_Z \frac{1}{\varepsilon_i}}, \quad \text{where } \varepsilon_i=\varepsilon_\parallel\cos^2\theta+\varepsilon_\perp\sin^2\theta, \tag{8}$$

where $N_X$ is the number of lattice points in the $x$ direction, $N_Z$ is the number of lattice points in the $z$ direction, and $\theta$ is the angle between the director and the $z$ axis. For the measured data, the effective dielectric constant was calculated using Eq. (7), while Eq. (8) gave the value for the simulations.

For the planar sample, the $X$-$Z$ plane is different from the $Y$-$Z$ plane because of the directional nature of the boundary conditions induced by the direction of rubbing. To include this effect, the simulations were performed in both planes and the effective dielectric constant was averaged. The calculated director configurations had no significant differences, probably due to the fact that the $d/P_0$ ratio is quite large.

As noted above, the rotational viscosity for the simulation must be adjusted to take into account the high percentage of chiral. It was found that a good fit was obtained if the rotational viscosity (which scales time) was reduced by a factor of 3.3. This shift can be explained by the fact that adding a large amount of CB15 (which is isotropic at room temperature) lowers the transition temperature [14], thus effectively bringing the system closer to the transition, and thereby reducing the viscosity. The rotational viscosity drops by approximately a factor of 2 every 10 °C [14]. This suggests that the transition temperature dropped by about 17 °C, agreeing well with the reduction found based on elastic constant reduction. Therefore, we renormalized time for the homeotropic simulation data using $t_{\mathrm{new}}=t_{\mathrm{old}}/3.3$. For planar boundary conditions, the initial director configuration contained a small twist-splay region at the surfaces as shown in Fig. 2(a). The thickness of this layer can be calculated using Eq. (9) [15]. The $\theta_0$ in the coefficient of Eq. (9) is the polar pretilt angle in degrees. In this study, this was $90°-3.75°=86.25°$.

$$\theta(x)=\left(\frac{\theta_0}{90°}\right)2\arctan[e^{-x/\xi_E}], \quad \xi_E=\frac{1}{E}\left(\frac{K_{\mathrm{AVG}}}{\Delta\varepsilon\varepsilon_0}\right)^{1/2}. \tag{9}$$

The average dielectric constant as a function of time for the two samples is shown in Fig. 5. The reader will note that the average dielectric constant for homeotropic boundary conditions is held for a short time in the $H$ state, while the planar sample starts relaxing immediately. The curves for both boundary conditions reach a minimum slightly after 1 ms. The fact that, at this minimum, the value of the average dielectric constant is close to the value of $\varepsilon_\perp$ implies a director configuration where the average polar angle of the director is close to 90°. This condition is satisfied by the TP state. However, the experimental results do not show the TP state being as ''perfect.'' This could be caused by any combination of the following factors. The Helfrich-like distortions do not occur in the model unless there is noise. If noise were added differently, this could influence the TP state. The given values of the elastic constants when CB15 is mixed at 40% with MLC 6080 are only approximate. A shift in the $K_{33}/K_{22}$ ratio could also affect this state. Finally, the fact that the simulation is restricted to two spatial dimensions

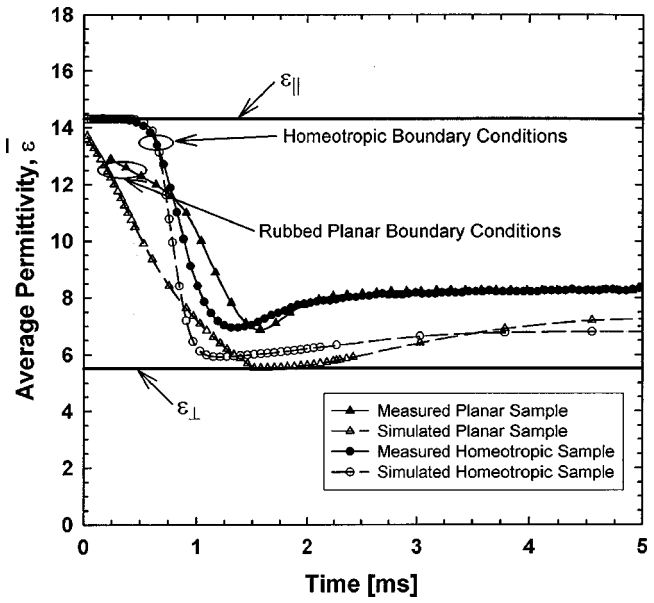


FIG. 5. Dynamics of the effective dielectric constant for both samples. The solid lines and symbols represent the experimental results, while the dashed lines and open symbols show the simulation results. Notice that the data for the homeotropic sample are held in the homeotropic state briefly.

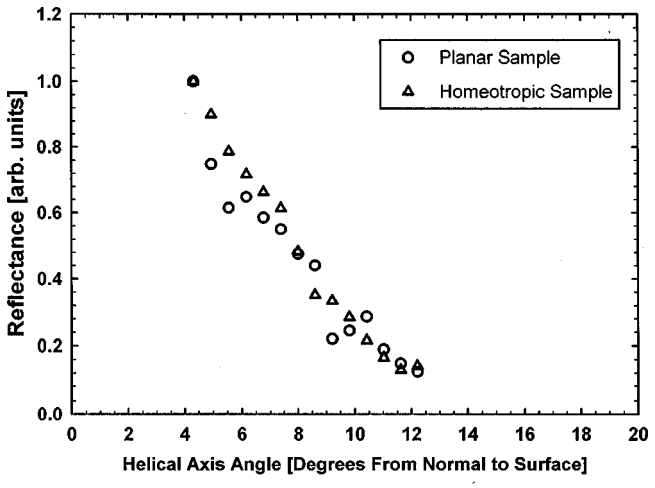


FIG. 6. Measured helical axis distribution for the transient planar state in both samples. The sharp decrease in reflecting helices indicates the transient planar state is a ''perfect'' state.

might also play a role. Work is currently underway to match the experiment with the experiment better.

In the second experimental apparatus, collimated monochromatic light was incident on the sample at an angle $\alpha$ from the substrate normal direction. Only light reflected directly back along the incident light direction (with an angular precision of roughly 3°) was measured [12]. Because light reflected at oblique angles from cholesteric helices was not measured in our setup, the measured reflected signal is directly related to the density of reflecting helices with axes making an angle $\alpha$ with the substrate normal and with pitch in the range $\lambda/n_c$ to $\lambda/n_o$, where $\lambda$ is the vacuum wavelength of light. Thus we can measure the spectrum as a function of time to experimentally confirm the existence of the TP state [12]. By varying the angle $\alpha$, we can obtain information on the orientation of the reflecting helices in the TP state. Snell's law can be used to relate this angle $\alpha$ to the angle of the helix, $\theta$. Figure 6 shows the measured helical axis distribution for both samples. This figure clearly shows that, for both cases, the transient planar state is approximately a perfect state, having nearly all its helical axes aligned perpendicular to the substrates.

To calculate the optical transmittance of the simulated two-dimensional director configurations correctly, a multidimensional numerical solution of Maxwell's equations would ensure accuracy [16]. However, this is exceedingly computer intensive [16]. For this reason, we decided to develop a program which would convert the director configuration into a series of helical structures oriented along various axes, and determine the reflective properties of the calculated director indirectly through comparison with Berreman $4\times4$ calculations [17] of reflections from helices of various degrees of twist.

In order to determine the helical components of a director configuration along a given incident light direction, the following procedure was implemented. First, the approximate direction of the light travel through the material was determined from Snell's law. Next, a series of light paths through the sample was plotted, with a light path originating at each lattice point along the $z=0$ substrate. At each point where the light path intersected a horizontal lattice line, the director was calculated through a linear extrapolation from the points nearest the intersection. A coordinate transformation was then applied to the determined director at each intersection such that the light vector became the $z$ direction. The resultant series of new directors along each light path was then set up as a column in a new director configuration. The $z$-lattice spacing of the new director configuration was increased to account for the longer distance light must travel to traverse the sample obliquely.

At this point, a representation of the director as seen by light incident at an oblique angle was obtained. In order to determine the presence of helical axes along this light direction, director elements that were not approximately perpendicular to the incident light direction (that is, the new $z$ direction) were eliminated. The allowance condition for a director element to be perpendicular was that it was titled away from the light-normal plane by less than 3°. A value of 3° was chosen because the measured divergence of the incident light beam in the retro-reflection apparatus was about 5°, which adjusted for refraction gives a 3° light cone inside the light crystal.

With only helical components approximately parallel to the light path remaining, it was necessary to develop a method for analyzing individual helices. For each helix, the pitch and degree of twist was determined from the modified director structure. Based on this pitch and twist, a distribution of reflections at various wavelengths was determined from a look-up table. The table was developed by calculating the reflections at various wavelengths from cholesteric helices of varying twist. In order to compare the resulting data directly to the measured retroreflection data from experiment, an array of bins of width 25 nm ranging from 375 to 1100 nm was used. For every helix, the degree of reflection

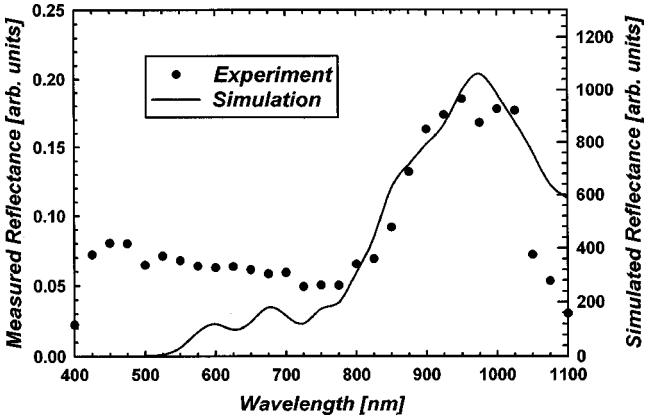


FIG. 7. Measured and simulated reflectance spectrum for the transient planar in the planar sample.

at percentages of the central reflective wavelength from 60% to 140%, with a step size of 1%, were placed into the corresponding bins.

Because we are only calculating the nearly on axis optics for the nearly uniform TP state, this approximation is very good. Figure 7 shows the measured and simulated reflectance during the TP state for the rubbed planar sample. Figure 8 shows the reflectances for the TP state in the homeotropic sample. The experimental spectra in these figures were obtained with an angle $\alpha$ of 7°. This is the smallest value we could obtained without measuring specular reflection from the glass-air interface. The experimental and calculated curves agree very closely for the rubbed planar sample; however, the difference between the experiment and simulation for the homeotropic boundary condition suggests that the values of the $K_{33}/K_{22}$ elastic constant ratio assumed in simulation is larger than in experiment. The peak in the blue is probably due to multiple off-axis reflections. This would cause a blueshifting of the wavelength of reflected light [1].

Third, we connected an Oriel flash lamp to a Nikon Optiphot-2 polarizing microscope. The flash lamp is triggered by a delay box, which delays the trigger from a Stanford Research Model DS345 Function Generator. The measured duration of the flash is approximately 9 ns. This ensures that we obtain clear pictures at precisely the time we desire. These photos are shown in Figs. 9 and 10. The photographs of times before 1.25 ms for the planar sample and 1.0 ms for the homeotropic sample were too dark to be developed, suggesting there were no domains present. Also, the significant increase in domain density from 1.25 to 1.5 ms for the planar sample, and 1.0 to 1.25 ms for the homeotropicsample imply that domains start to form at roughly 1.13

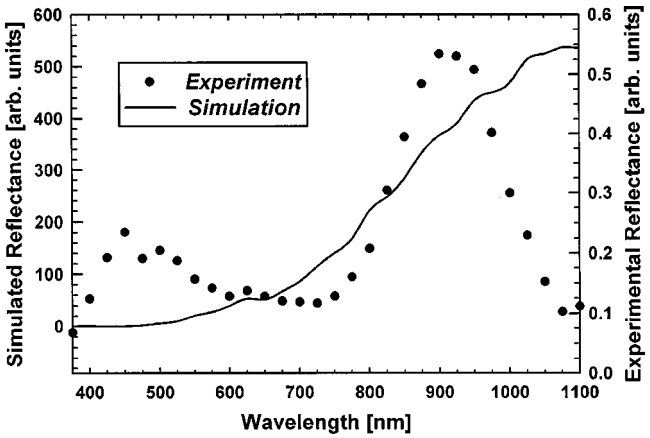


FIG. 8. Measured and simulated reflectance spectrum for the transient planar in the homeotropic sample.

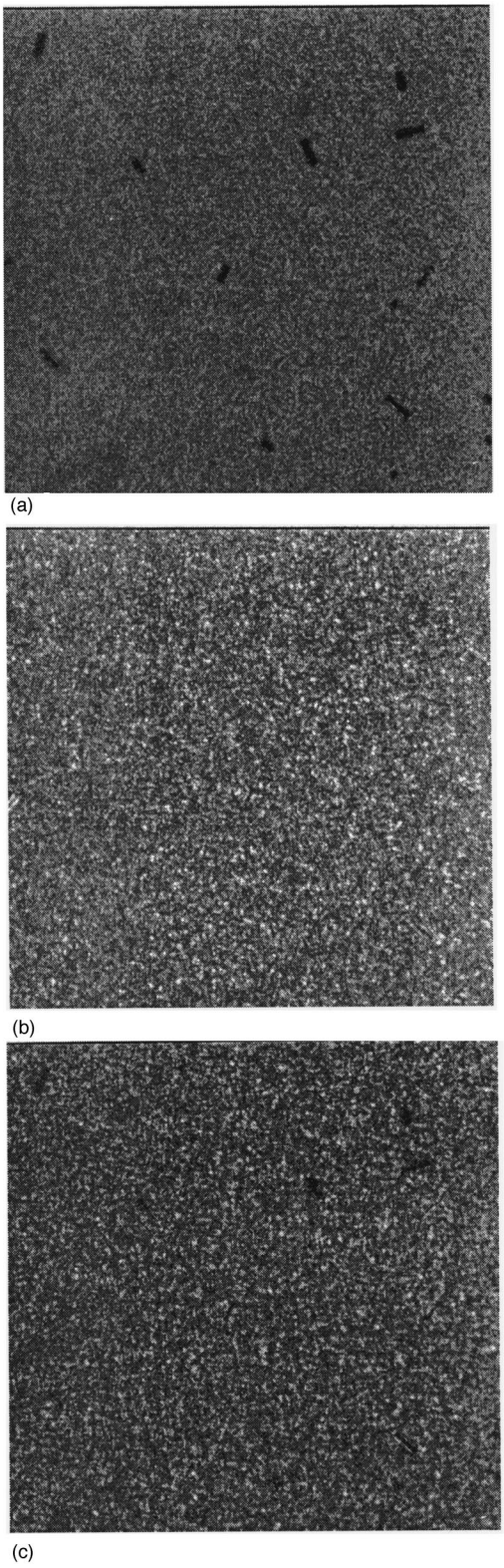


FIG. 9. Microscope photographs of the textures in the planar sample. Times are (a) 1.25, (b) 1.5, and (c) 2.0 ms.

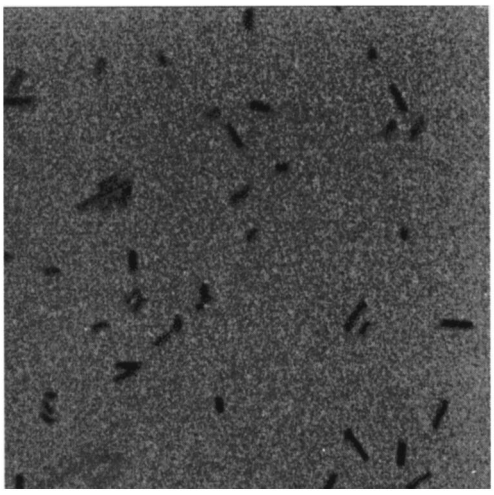

(a)

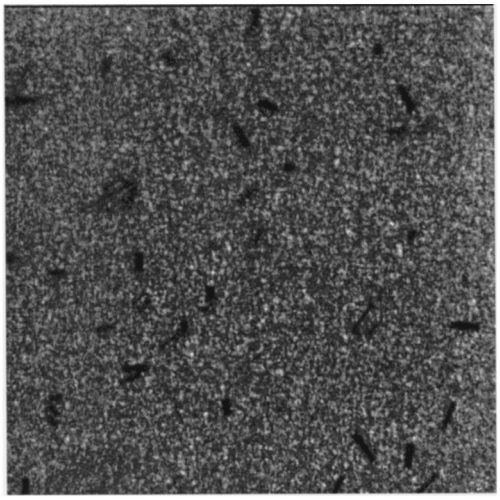

(b)

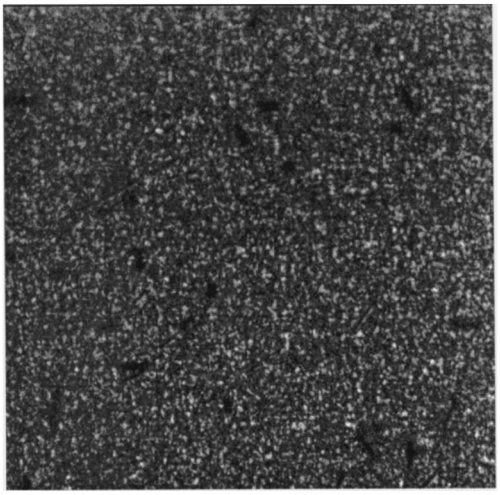

(c)

FIG. 10. Microscope photographs of the textures in the homeotropic sample. Times are (a) 1.0, (b) 1.25, and (c) 1.5 ms.

ms for the planar sample and 0.83 ms for the homeotropic sample. The simulations show the onset of a periodic structure that eventually leads to domains starting at approximately the same times.

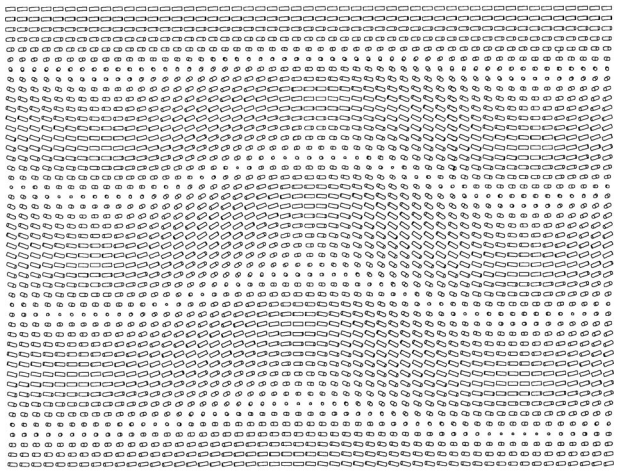

FIG. 11. Close up of Helfrich-like undulation distortion in the transition from the transient planar state to the focal conic state in the planar sample. All calculated data points are shown.

## IV. DISCUSSION

The numerical simulations show the directors dropping to the TP state on the way from the *H* state to the FC state for the values of applied voltage used here for both planar and homeotropic boundary conditions. This transition to the TP state is accomplished via a one-dimensional conical relaxation. It has been theoretically suggested that the pitch of the TP state should be $K_{33}/K_{22}P_0$ [4]. For our system, this quantity evaluates to $800.2 \pm 13.8$ nm. The pitch of the TP state found in experiment is $609.2 \pm 6.2$ nm for the planar sample, suggesting that the pitch does wind up somewhat during this conical relaxation. The pitch is more difficult to measure in the homeotropic sample because the reflectance peak is not as sharp, but can be estimated at $563.3 \pm 62.0$ nm. The simulations give the pitch in the bulk to be $612.2 \pm 12.7$ nm for the planar sample and $714.3 \pm 62.0$ nm for the homeotropic sample, agreeing very well with experiment. The large uncertainty for the homeotropic sample is due to the distribution of pitches in the sample. The discrepancy in the homeotropic data could be caused by errors in the elastic constants used in simulation. This is not a problem for the planar sample, where the boundary conditions force the system into an integer number of turns. Therefore, we now have quantitative numerical evidence that the director configuration responsible for the reflectance peak at longer wavelengths and the minimum in the capacitance curve during the transition from the *H* state to the FC state is indeed the TP state.

The simulations suggest that the TP state grows in from the surfaces for planar boundary conditions and from the bulk for homeotropic boundary conditions. This agrees with Mi and Yang, who performed a one-dimensional simulation of the transition from the *H* state to the TP state to the *P* state [18].

Our preliminary calculations for the latter part of the transition suggest that the TP state transforms to the FC state through a Helfrich-like undulation distortion [19]. Figure 11 shows a close-up of such a place in the calculation with rubbed planar boundary conditions. This is very similar to what we have recently found for the transformation process from the TP state to the *P* state [20]. This distortion during

the transition from the TP state to the FC state grows from the surface in the planar sample, while in the homeotropic sample, it grows from the bulk (see Figs. 2 and 3).

## V. CONCLUSIONS

In this paper, we have shown quantitative numerical modeling of the transition from the *H* state to the FC state that shows the existence of the TP state and agrees well with measured data. Previous experimental evidence has suggested the existence of this state; however, it did not appear to be physically reasonable. We compared this simulation with two experimental samples: one with parallel boundary conditions and one with perpendicular boundary conditions. The agreement of the simulation with the experimental data indicates that it is indeed energetically preferable for the system to pass through the TP state during the transition from the *H* state to the FC state. Also shown here are preliminary results for the second part of the transition, suggesting that the transition from the TP state to the FC state starts via a Helfrich-like undulation distortion.

## ACKNOWLEDGMENTS

This work was supported under NSF ALCOM grant No. DMR 89-20147 and DARPA N61331-96-C-0042.

[1] P. G. de Gennes and J. Prost, *The Physics of Liquid Crystals* (Oxford University Press, New York, 1993).
[2] D. Davis, A. Kahn, X. Y. Huang, and J. W. Doane, SID Dig. Tech. Pap. **29**, 901 (1998).
[3] W. Greubel, Appl. Phys. Lett. **25**, 5 (1974).
[4] D.-K. Yang and Z.-J. Lu, SID 95 Dig. Tech. Pap. **26**, 351 (1995).
[5] J. E. Anderson, P. Watson, and P. J. Bos, SID Dig. Tech Pap. **30**, 198 (1999).
[6] D. W. Berreman, Appl. Phys. Lett. **25**, 12 (1974).
[7] S. Dickmann, J. Eschler, O. Cossalter, and D. A. Mlynski, SID Dig. Tech. Pap. **24**, 638 (1993).
[8] Hiroyuki Mori, Eugene C. Gartland, Jr., Jack R. Kelly, and Philip J. Bos, Jpn. J. Appl. Phys. **38**, 135 (1999).
[9] I. Fedak, R. D. Pringle, and G. H. Curtis, Mol. Cryst. Liq. Cryst. **82**, 173 (1982).
[10] Information supplied by Merck.
[11] L. M. Blinov and V. G. Chigrinov, *Electrooptical Effects in Liquid Crystal Materials* (Springer-Verlag, New York, 1994).
[12] P. Watson, V. Sergan, J. E. Anderson, J. Ruth, and P. J. Bos, Liq. Cryst. **26**, 731 (1999).
[13] X.-Y. Huang, Ph.D. Thesis, Kent State University, 1996.
[14] W. H. DeJeu, *Physical Properties of Liquid Crystalline Materials* (Gordon and Breach, New York, 1980).
[15] E. B. Priestley, Peter J. Wojtowicz, and Ping Sheng, *Introduction to Liquid Crystals* (Plenum Press, New York, 1975).
[16] C. M. Titus, P. J. Bos, and J. R. Kelly, SID Dig. Tech Pap. **30**, 624 (1999).
[17] D. W. Berreman, J. Opt. Soc. Am. **62**, 502 (1972).
[18] Xiang-Dong Mi and Deng-Ke Yang, SID 98 Dig. Tech. Pap. **29**, 909 (1998).
[19] W. Helfrich, Appl. Phys. Lett. **17**, 531 (1970).
[20] P. Watson, J. E. Anderson, V. Sergan, and P. J. Bos, Liq. Cryst. **26**, 1307 (1999).